Applied Surface Science 257 (2011) 7221–7225

Contents lists available at ScienceDirect

Applied Surface Science

journal homepage: www.elsevier.com/locate/apsusc

# Structure and refractive index dispersive behavior of potassium niobate tantalate films prepared by pulsed laser deposition

Wenlong Yang, Zhongxiang Zhou*, Bin Yang, Yongyuan Jiang, Hao Tian, Dewei Gong, Hongguo Sun, Wen Chen

*Department of Physics, Harbin Institute of Technology, Harbin 150001, PR China*

ARTICLE INFO

*Article history:*
Received 26 January 2011
Received in revised form 11 March 2011
Accepted 15 March 2011
Available online 23 March 2011

*Keywords:*
Potassium niobate tantalate film
Pulsed laser deposition
Structure
Refractive index dispersion
Sellmeier oscillator approximation

ABSTRACT

Pure perovskite phase and crack-free $KTa_{0.5}Nb_{0.5}O_3$ thin films were prepared on Pt/Ti/$SiO_2$/Si substrates by pulsed laser deposition. The structure and orientation were analyzed by X-ray diffraction. The optical properties were investigated by an ellipsometer. The relationship between the refractive index dispersive behavior and internal structure was analyzed by Sellmeier dispersion model and single electronic oscillator approximation. The parameters of room temperature monomial Sellmeier oscillator were calculated. And the refractive index dispersive parameter $E_0/S_0$ of $KTa_{0.5}Nb_{0.5}O_3$ thin films on Pt/Ti/$SiO_2$/Si substrates is $(6.72 \pm 0.04) \times 10^{-14}$ eV $m^2$, which is consistent with those of KTN crystals and compounds with $ABO_3$ perovskite type structure.



## 1. Introduction

Potassium niobate tantalate, $KTa_{1-x}Nb_xO_3$ (KTN), has received a great deal of attention due to its remarkable ferroelectric, dielectric, photorefractive, electro-optical and nonlinear-optical properties [1–6]. Because KTN is a compatible solid solution of potassium tantalite ($KTaO_3$) and potassium niobate ($KNbO_3$), the phase structures and the properties can be modulated by controlling the composition, and the Curie temperature of paraelectric–ferroelectric phase transition varies with the Ta/Nb ratio [5,7]. In last decades, KTN single crystals have been widely investigated owing to their excellent potential for optical device performance as their large quadratic electro-optic effect. The electro-optic coefficient is about 20 times larger than that of conventional $LiNbO_3$ [8]. However, single crystal KTN is considered impractical for applications, because it is difficult to grow large and good quality KTN crystals [9].

KTN thin film appears much more suitable for optical devices as well as some another applications, since not only the problems of compositional gradient and inhomogeneity, but also the process of cutting and polishing can be avoided [10]. Many methods have been used for preparing KTN films, such as sol–gel deposition [9,11,12], chemical solution deposition (CSD) [13,14], metal organic chemical vapor deposition (MOCVD) [15,16], magnetron sputtering [17] and pulsed laser deposition (PLD) [10,18–20]. Pure or dominating perovskite phase and oriented KTN films have been successfully grown on Si [14,21], (1 0 0) MgO [13,18,19], (1 0 0) and (1 1 0) $SrTiO_3$ [9,10,12], platinum coated silicon [17] and sapphire substrates [19]. Besides the substrates match, another key issue of KTN preparation is K compensation, as K deficiency tends to promote the formation of pyrochlore phase [20]. The study about optical properties of KTN films is also one of the investigative hotspots, and the optical and nonlinear properties have been reported previously [6,18,22]. However, rare studies about refractive index dispersive behavior have been reported.

In this paper, $KTa_{0.5}Nb_{0.5}O_3$ thin films were grown on Pt/Ti/$SiO_2$/Si substrates by PLD technique and K enriched KTN ceramic targets were used. The structure, orientation and optical properties of the films were investigated. The relation between the refractive index dispersive behavior and internal structure was analyzed by Sellmeier dispersion model and single electronic oscillator approximation.

## 2. Experimental procedure

$KTa_{0.5}Nb_{0.5}O_3$ (KTN50) thin films were grown on Pt/Ti/$SiO_2$/Si substrates by PLD technique. K enriched KTN ceramic targets were prepared by traditional solid state reaction. A KrF excimer laser (LPX205i, Lambda Physik, 248 nm) was used as the irradiation source; the pulse energy fluence and target–substrate distance were set at 2.0 J/$cm^2$ and 6 cm, respectively. The deposition of thin

* Corresponding author. Tel.: +86 451 8641 4130.
*E-mail address:* zhouzx@hit.edu.cn (Z. Zhou).

0169-4332/$ – see front matter © 2011 Elsevier B.V. All rights reserved.
doi:10.1016/j.apsusc.2011.03.094

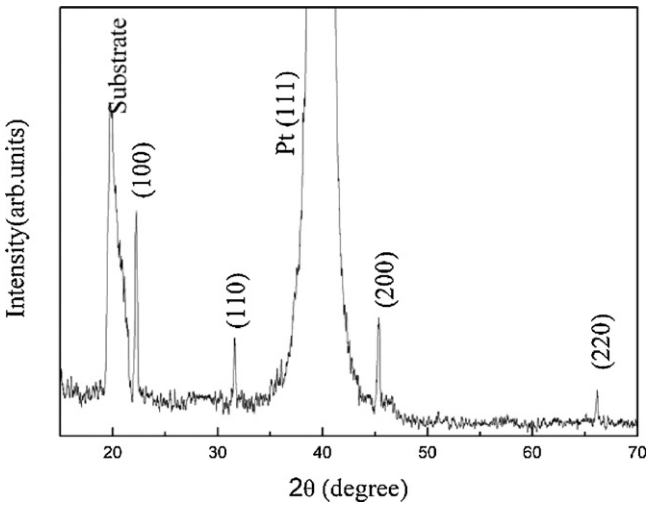


**Fig. 1.** Room temperature X-ray diffraction patterns of KTN50 films grown at 700 °C on Pt/Ti/$SiO_2$/Si substrates.

films was performed in the chamber with 15 Pa oxygen atmosphere and the substrates temperature of 700 °C for 30 min. Then, the films were annealed in situ at the same temperature with 30 Pa oxygen pressure for 10 min.

K enriched KTN ceramic targets were prepared with high-purity (99.99%) potassium carbonate ($K_2CO_3$), niobium oxide ($Nb_2O_5$) and tantalum oxide ($Ta_2O_5$) as raw materials. In order to compensate the severe K loss in the process of thin films growth, 60% (atomic) $K_2CO_3$ excess was added in the stoichiometric mixtures. After being mixed, milled and synthesized at 650 °C for 4 h, the calcined powders were pressed into cylindrical pellets of 30 mm diameter and about 5 mm thick. Then, the compact K enriched KTN ceramic targets were achieved by 4 h sintering at 1000 °C.

The crystal phase structures were monitored by X-ray powder diffraction (XRD-6000, Shimadzu, Japan) with Cu Kα radiation. The microstructures were studied by scanning electron microscopy (SEM, S-4700, Hitachi, Japan) and the surface topographies were detected by scanning probe microscopy (SPM, CSPM500, Ben Yuan Ltd., China). The optical property measurements were performed on an ellipsometer (α–SE™, J.A. Woollam Co., Inc., American).

## 3. Results and discussion

### 3.1. Structure characterization of KTN films

Fig. 1 shows the room temperature XRD patterns of the films grown at 700 °C on Pt/Ti/$SiO_2$/Si substrates. According to the results of crystallographic indexing, KTN films present a perovskite type $ABO_3$ subcell. As shown in Fig. 1, the films possess tetragonal symmetry and no second phase is observed. The lattice parameters $a$ and $c$ of the KTN50 films were calculated, and the values are 3.993 and 4.020 Å, respectively. The (1 0 0), (1 1 0), (2 0 0), (2 2 0) peaks appear with certain intensities, which are in good agreement with those of the targets. The films contain both (1 0 0) and (1 1 0) orientations, while the targets exhibit a random orientation as expected. The degree of (1 0 0) orientation of the films can be estimated by the Lotgering factor from the XRD data [23–25].

$$f(l00) = \frac{P(l00) - P_0}{1 - P_0}$$

$$P(l00) = \frac{\sum I(l00)}{\sum I(hkl)}$$

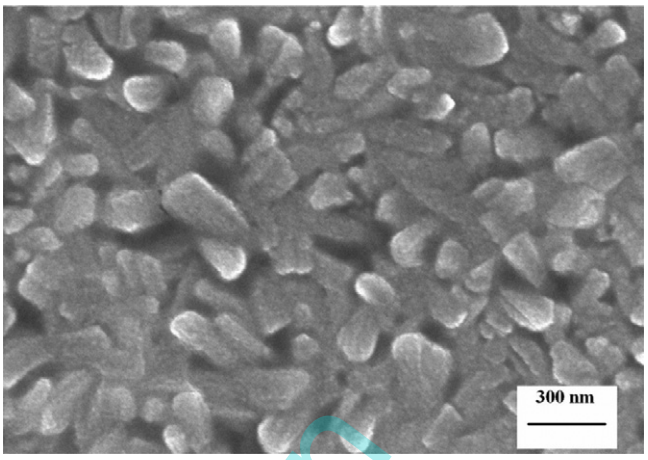


**Fig. 2.** Scanning electron micrograph (SEM) of KTN50 films grown at 700 °C on Pt/Ti/$SiO_2$/Si substrates.

$$P_0 = \frac{\sum I_0(l00)}{\sum I_0(hkl)}$$

where $\sum I(l00)$ and $\sum I(hkl)$ are the summations of the XRD peak intensities of all the $(l00)$ peaks and all $(hkl)$ peaks in the oriented film, respectively. $\sum I_0(l00)$ and $\sum I_0(hkl)$ are the summations of the XRD peak intensities of all the $(l00)$ peaks and all $(hkl)$ peaks in the randomly oriented sample, respectively. The value of Lotgering factor varies from 0 (completely random) to 1(perfectly oriented). The factor of the film grown at 700 °C is calculated for a $2\theta$ scan between 20° and 70°, and the value is 62%. The (1 0 0)-oriented degree in our case is of the middle order with KTN films grown on other substrates [26]. The selections of substrates and growth conditions are ascribed to the orientation. The influence of the substrate depends on both lattice matching and chemical bonding between the substrates and the films [12]. In our case, Pt/Ti/$SiO_2$/Si substrates are selected, and the mismatch is about 2% for KTN on Pt, which is small and favorable for the formation of orientating films [26]. At the same time, the growth temperature and oxygen pressure are also important factors [27].

### 3.2. Microstructure and the surface topography of KTN films

The SEM image of the KTN50 films on Pt/Ti/$SiO_2$/Si substrates is shown in Fig. 2. The films are crack-free and homogeneous with quite uniform grains, and the grain size is about 100 nm × 200 nm. It can be seen from the images that the films have dense microstructure and well crystalline quality. This can be explained by the small mismatch between KTN and Pt substrates, and the high migration energy of the particles from the plasma produced by the impact of the high energy pulse laser onto the target. The SPM (2D and 3D) surface images of the films deposited at 700 °C for 30 min are shown in Fig. 3. The images are characterized by slight surface roughness with a uniform crack-free densely packed microstructure, which corresponds with the results of SEM. A random area about 23.818 μm × 23.818 μm was chosen for surface roughness analyzing. The surface roughness parameters of the films are calculated by the equipment's software routine method. The values of surface roughness average (RA) and root mean square (RMS) for the films are 17.7 nm and 22.6 nm, respectively. The values of surface roughness are of the same order with the reports for KTN films [27].

### 3.3. Refractive index dispersive behavior of KTN films

The optical property measurement was performed on an ellipsometer. The angle of the incident light is 70°. The amplitude $\psi$

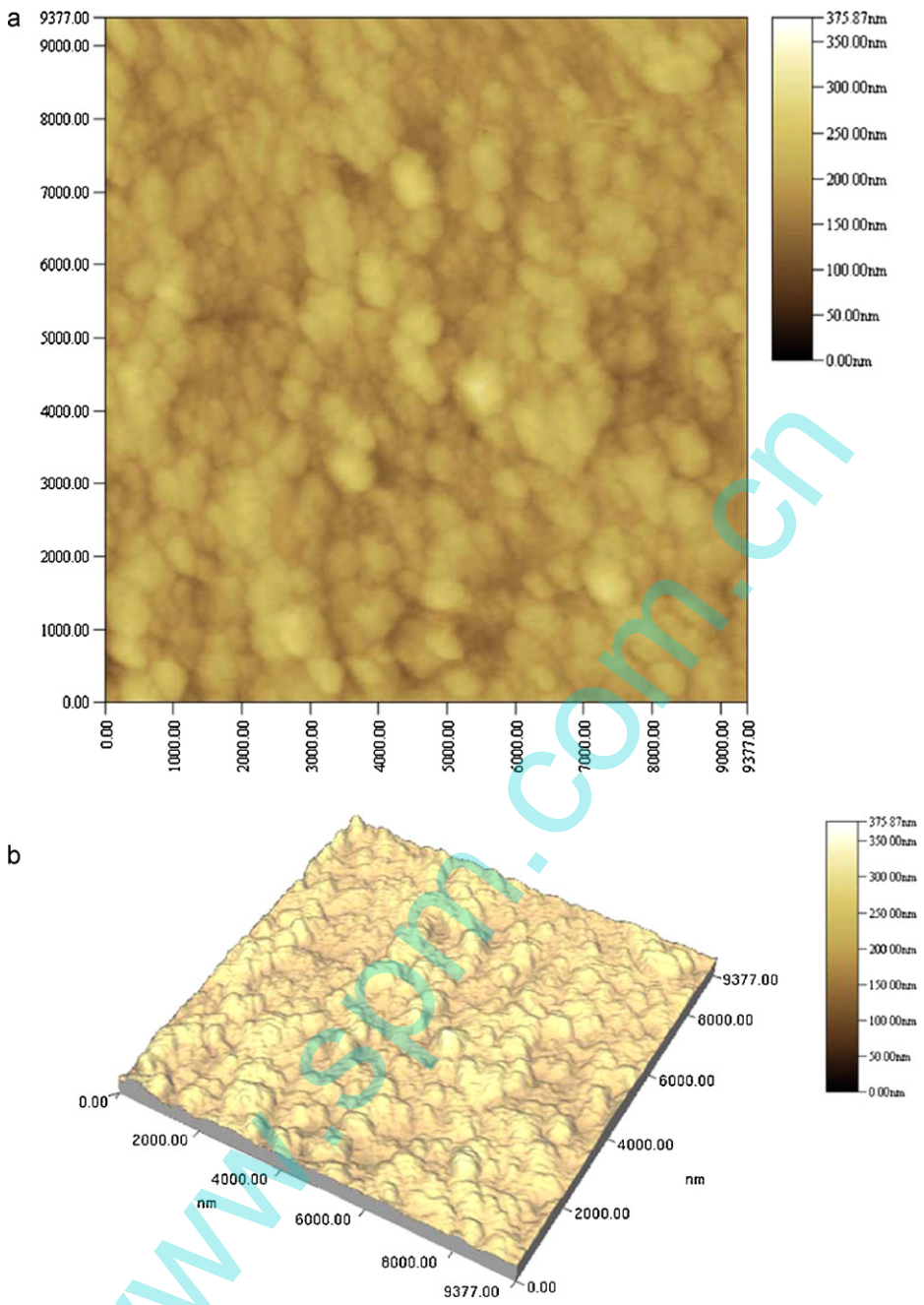


**Fig. 3.** Scanning probe microscopy 2D (a) and 3D (b) surface topographies of KTN50 films grown at 700 °C on Pt/Ti/$SiO_2$/Si substrates.

and phase $\Delta$ information of the emergent light of KTN50 films on Pt/Ti/$SiO_2$/Si substrates in the wavelength range from 380 nm to 900 nm are shown in Fig. 4, respectively. The experiment data were analyzed as the Pt layer is thick enough and the incident light could not penetrate through the Pt layers [28].

The thickness of the KTN50 films grown at 700 °C on Pt/Ti/$SiO_2$/Si for 30 min calculated from the ellipsometer is 120 nm, which is consistent with SEM observation for cross-sections of the thin films. The refractive indexes $n$ and the extinction coefficients $k$ of the KTN50 films on Pt/Ti/$SiO_2$/Si substrate in the wavelength range from 380 nm to 900 nm are shown in Fig. 5, which are derived from the experimental results of the ellipsometer. The wavelength dependence refractive indexes show the typical shape of a normal dispersion curve. It can be seen from the figure that the refractive index $n$ and extinction coefficient $k$ of the KTN50 films decrease with the increase of wavelength from 380 nm to 900 nm. The extinction coefficient $k$ is very small when the wavelength is longer than 600 nm, where the films are nearly transparent. When wavelength is shorter than 400 nm, the extinction coefficient $k$ becomes bigger. The possible reason is that the wavelength approaches to KTN materials' absorption band of near 370 nm [29]. The refractive index of the films measured by ellipsometer is close to the bulk value [5,18,30], as shown in Table 1. The results confirm the high

**Table 1**
Room temperature refractive indexes of KTN materials at different wavelength.

| Wavelength (nm) | 546.1 | 589.3 | 632.8 |
|---|---|---|---|
| $KTa_{0.5}Nb_{0.5}O_3$ films | 2.303 | 2.289 | 2.279 |
| $KTa_{0.5}Nb_{0.5}O_3$ films on MgO [18] | – | – | 2.2396 |
| $KTa_{0.65}Nb_{0.35}O_3$ crystals [5] | 2.323 | 2.302 | 2.286 |
| $KTa_{0.48}Nb_{0.52}O_3$ crystals [30] | 2.324 | 2.301 | 2.284 |

**Table 2**
Room temperature monomial Sellmeier parameters of single oscillator approximation.

| Materials | $\lambda_0$ (nm) | $S_0$ ($\times 10^{14}$ m$^{-2}$) | $E_0$ (eV) | $E_d$ (eV) | $E_0/S_0$ ($\times 10^{-14}$ eV m$^2$) |
|---|---|---|---|---|---|
| $KTa_{0.5}Nb_{0.5}O_3$ films | 200.4 ± 0.6 | 0.919 ± 0.005 | 6.18 ± 0.02 | 22.84 ± 0.07 | 6.72 ± 0.04 |
| $KTa_{0.65}Nb_{0.35}O_3$ crystals [5] | – | 0.94 | 6.17 | 23.4 | 6.6 |

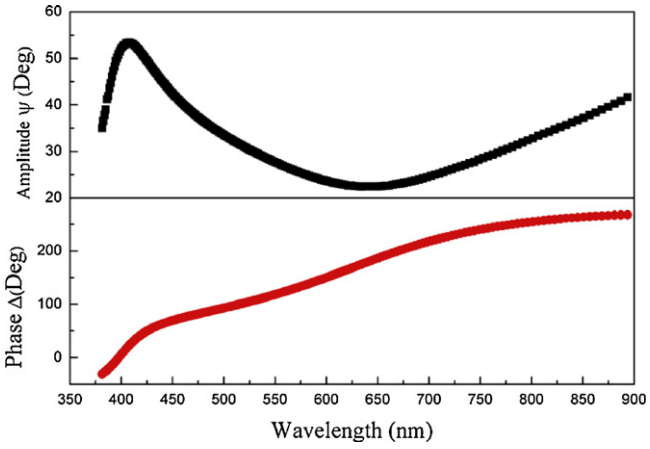


**Fig. 4.** Amplitude and phase information of the emergent light of KTN50 films from the ellipsometer.

quality of the KTN films, as is well known that the refractive index is strongly influenced by the crystallization, density, electronic structure and the defects of the films [20,31].

It can be seen that KTN50 films possess significant dispersive behavior range from 380 nm to 900 nm in wavelength. The dispersive behavior is similar with that of compounds with $ABO_3$ perovskite type structure, such as PT, BZT, BTO and STO, because of the similar structure [28,31,32]. It is well known that the frame of $ABO_3$ structure is $BO_6$ oxygen octahedron, which is closely related to the wavelength dependent refractive dispersion. The dispersive behavior of KTN50 films could be described by Sellmeier dispersion formula [33,34]:

$$n^2 = A + \frac{B}{\lambda^2 - C} + D\lambda^2$$

where $A$, $B$, $C$ and $D$ are Sellmeier parameters, and the values calculated by experimental curve fitting are 4.831 ± 0.004, 0.0932 ± 0.008 μm$^2$, 0.0728 ± 0.0005 μm$^2$ and −0.202 ± 0.005, the related coefficient of the fitting curve is bigger than 99.98%, as seen the solid line shown in Fig. 5. In order to stress the importance

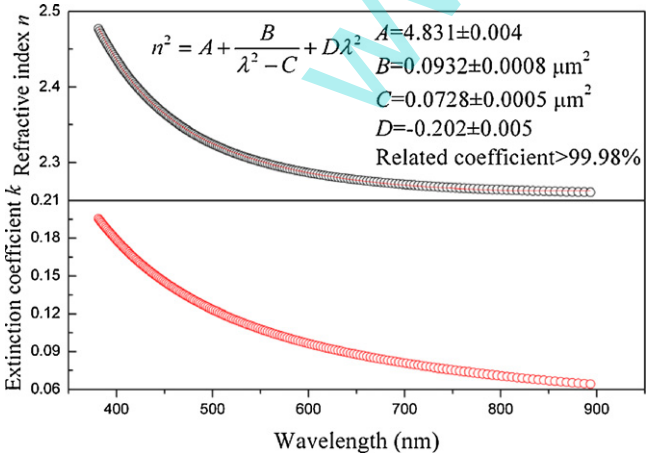


**Fig. 5.** Optical constants (circle dots) and Sellmeier dispersion formula (solid line) of KTN50 films grown at 700 °C on Pt/Ti/$SiO_2$/Si substrates.

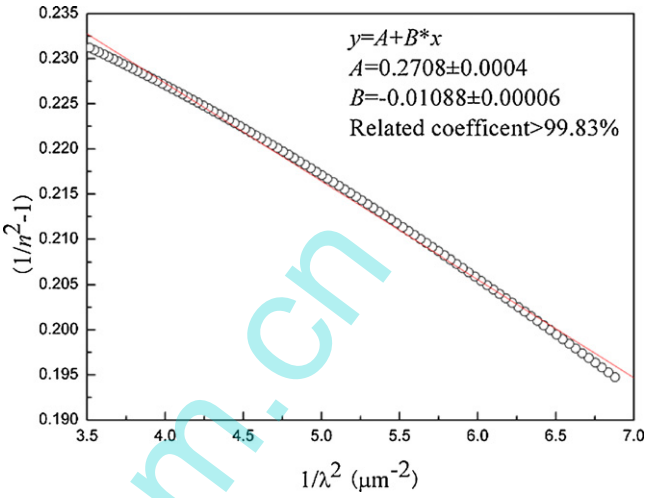


**Fig. 6.** Plot of refractive index factor $(n^2 - 1)^{-1}$ versus $\lambda^{-2}$ for KTN50 films.

of the basic $BO_6$ oxygen octahedron building block in this class of materials, Didomenico and Wemple (R) improved the monomial Sellmeier dispersion formula and related the optical properties to internal structure by single electronic oscillator approximation

$$n^2 - 1 = \frac{S_0\lambda_0^2}{1 - (\lambda_0/\lambda)^2} = \frac{E_d E_0}{E_0^2 - E^2}$$

where $\lambda$ and $E$ is the wavelength and energy of the incident light, respectively; $\lambda_0$ is the average oscillator position and $S_0$ is the average oscillator strength; $E_d$ is the dispersive energy and $E_0$ is the energy of the single oscillator. These parameters were calculated from the relationship between $1/(n^2 - 1)$ and $\lambda^{-2}$, as shown in Fig. 6. An acceptable linear fit is found, but some deviations are also observed. The defects may be an important reason, because the microporosities and oxygen vacancies are unavoidable in the preparation of the thin films; the depolarization of the incident light by grain boundary morphologies is also a possible reason; in addition, the absorption of the thin films may affect the experimental parameters and deteriorate the fitting [28]. The results of the calculated parameters are shown in Table 2. The refractive index dispersive parameter $E_0/S_0$ is one of the important parameters to describe the optical dispersion behavior in detail. Didomenico and Wemple [33] take for $E_0/S_0$ the specific experimental value of $(6 \pm 0.5) \times 10^{-14}$ eV m$^2$ for crystal. In our case, the refractive index dispersive parameter $E_0/S_0$ is $(6.72 \pm 0.04) \times 10^{-14}$ eV m$^2$. These similar parameters of KTN50 thin films grown on Pt/Ti/$SiO_2$/Si substrates and KTN crystal indicate the good crystalline quality of our films.

## 4. Conclusion

Pure perovskite phase and crack-free $KTa_{0.5}Nb_{0.5}O_3$ thin films were prepared on Pt/Ti/$SiO_2$/Si substrates by pulsed laser deposition. The structure and orientation were analyzed by X-ray diffraction. And the (1 0 0)-oriented factor of the film grown at 700 °C for a 2$\theta$ scan between 20° and 70° is 62%. The SEM and SPM images are characterized by slight surface roughness with a uniform crack-free densely packed microstructure. The optical

properties were investigated by an ellipsometer, and the relation between the refractive index dispersive behavior and internal structure was analyzed by Sellmeier dispersion model and single electronic oscillator approximation. The room temperature monomial Sellmeier oscillator parameters were calculated. The values of the average oscillator position $\lambda_0$, the average oscillator strength $S_0$, the energy of the single oscillator $E_0$ and the dispersive energy $E_d$ and are $200.4 \pm 0.6$ nm, $(0.919 \pm 0.005) \times 10^{14}$ m$^{-2}$, $6.18 \pm 0.02$ eV and $22.84 \pm 0.07$ eV, respectively. The refractive index dispersive parameter $E_0/S_0$ of $KTa_{0.5}Nb_{0.5}O_3$ thin films grown on $Pt/Ti/SiO_2/Si$ substrates is $(6.72 \pm 0.04) \times 10^{-14}$ eV m$^2$, which is consistent with those of KTN crystal and compounds with $ABO_3$ perovskite type structure and confirms the high quality of the KTN films.

## Acknowledgements

This work was supported by National Nature Science Foundation of China (no. 11074059). The authors wish to thank Materials Science and Engineering Center of Jilin Institute of Chemical Technology for providing the SPM characterization.

## References

[1] R. Pattnaik, J. Toulouse, Phys. Rev. Lett. 79 (1997) 4677.
[2] P.B. Ishai, C.E.M. de Oliveira, Y. Ryabov, Y. Feldman, A.J. Agranat, Phys. Rev. B 70 (2004) 132104.
[3] J.Y. Wang, Q.C. Guan, J.Q. Wei, Y.G. Liu, J. Cryst. Growth 116 (1992) 27.
[4] J.E. Geusic, S.K. Kurtz, L.G. Uitert, S.H. Wemple, Appl. Phys. Lett. 4 (1964) 141.
[5] F.S. Chen, J.E. Geusic, S.K. Kurtz, J.G. Skinner, S.H. Wemple, J. Appl. Phys. 37 (1966) 388.
[6] H.Y. Zhang, X.H. He, Y.H. Shih, K.S. Harshavardhan, L.A. Knauss, Opt. Lett. 22 (1997) 1745.
[7] S. Triebwasser, Phys. Rev. 114 (1959) 63.
[8] X.P. Wang, J.Y. Wang, H.J. Zhang, Y.G. Yu, W.L. Gao, R.I. Boughton, J. Appl. Phys. 103 (2008) 033513.
[9] C.J. Lu, A.X. Kuang, J. Mater. Sci. 32 (1997) 4421.
[10] S. Yilmaz, T. Venkatesan, R. Gerhar-Multhaupt, Appl. Phys. Lett. 58 (1991) 2479.
[11] A. Nazeri, Appl. Phys. Lett. 65 (1994) 295.
[12] A.X. Kuang, C.J. Lu, G.Y. Huang, S.M. Wang, J. Cryst. Growth 149 (1995) 80.
[13] K. Suzuki, W. Sakamoto, T. Yogo, S. Hirano, J. Am. Ceram. Soc. 82 (1999) 1463.
[14] J. Bursik, V. Zelezny, P. Vanek, J. Eur. Ceram. Soc. 25 (2005) 2151.
[15] A. Onoe, A. Yoshida, K. Chikuma, Appl. Phys. Lett. 78 (2001) 49.
[16] B.M. Nichols, B.H. Hoerman, J.-H. Hwang, T.O. Mason, B.W. Wessels, J. Mater. Res. 18 (2003) 106.
[17] S.R. Sashital, S. Krishnakumar, S. Esener, Appl. Phys. Lett. 62 (1993) 2917.
[18] A. Rousseau, M. Guilloux-Viry, E. Dogheche, M. Bensalah, D. Remiens, J. Appl. Phys. 102 (2007) 093106.
[19] A. Rousseau, V. Laur, S. Deputier, V. Bouquet, M. Guilloux-Viry, G. Tanne, P. Laurent, F. Huret, A. Perrin, Thin Solid Films 516 (2008) 4882.
[20] W. Peng, M. Guilloux-Viry, S. Deputier, V. Bouquet, Q. Simon, A. Perrin, A. Dauscher, S. Weber, Appl. Surf. Sci. 254 (2007) 1298.
[21] W.D. Ma, Z.S. Zhao, S.M. Wang, D.M. Zhang, D.S. Xu, X.D. Wang, Z.J. Chen, Phys. Status Solidi (a) 176 (1999) 985.
[22] L.A. Knauss, K.S. Harshavardhan, H.-M. Christen, H.Y. Zhang, X.H. He, Y.H. Shih, K.S. Grabowski, D.L. Knies, Appl. Phys. Lett. 73 (1998) 3806.
[23] F.K. Lotering, J. Inorg. Nucl. Chem. 9 (1959) 113.
[24] E.M. Sabolsky, S. Trolier-Mckinstry, G.L. Messing, J. Appl. Phys. 93 (2003) 4072.
[25] J. Wu, J. Wang, J. Am. Ceram. Soc. 93 (2010) 1422.
[26] Q. Simon, V. Bouquet, A. Perrin, M. Guilloux-Viry, Solid State Sci. 11 (2009) 91.
[27] L. Lu, D.Q. Xiao, Y. Sun, Y.B. Zhang, J.G. Zhu, Ferroelectrics 385 (2009) 8.
[28] A. Liu, J. Xue, X. Meng, J. Sun, Z. Huang, J. Chu, Appl. Surf. Sci. 254 (2008) 5660.
[29] Z. Keyu, Z. Duanming, Z. Zhicheng, Y. Fengxia, X. Han, Appl. Surf. Sci. 256 (2009) 1317.
[30] S. Loheide, S. Riehemann, F. Mersch, R. Pankrath, E. Kratzig, Phys. Status Solidi (a) 137 (1993) 257.
[31] S. Chopra, S. Sharma, T.C. Goel, R.G. Mendiratta, Appl. Surf. Sci. 236 (2004) 321.
[32] M. Cardona, Phys. Rev. 140 (1965) A651.
[33] M. Didomenico Jr., S.H. Wemple, J. Appl. Phys. 40 (1969) 720.
[34] S.H. Wemple, M. Didomenico Jr., Phys. Rev. B 3 (1971) 1338.